







Distributed Twist Sensing with Uncoupled Multi-Core Fibers Using Polarization-Sensitive Reflectometry

Arman Aitkulov [†], Martina Cappelletti[†] , Daniele Orsuti[†] , Luca Schenato, *Member, IEEE*, Tetsuya Hayashi, *Senior Member, IEEE*, Marco Santagiustina , *Member, IEEE*, Andrea Galtarossa , *Fellow, IEEE, Fellow, Optica*, and Luca Palmieri , *Senior Member, IEEE*.

Abstract—We explore the use of uncoupled multi-core fibers employed for telecommunications as a technological platform for implementing polarization-based distributed twist sensors. Through polarimetric-optical frequency domain reflectometry we assess the twist-induced birefringence along the cores of an uncoupled four-core fiber. By applying controlled twist, we show that the elasto-optic coefficient in each core is consistent with the value reported for single-mode fibers, and that the cores experience the same birefringence variations in response to the applied twist. Moreover, we leverage the distinctive birefringence properties of unspun uncoupled multi-core fibers to achieve long-range twist sensing, showing that the measured twist is in excellent agreement with the applied one even when the perturbed fiber location is 500-m away from the source. We achieve a remarkable accuracy of 4 degrees in measuring the angle by which the fiber is twisted, with a spatial resolution of 8 cm. These results support the potential of uncoupled multi-core fibers to realize twist sensors that are relevant for applications such as umbilical cable monitoring.

Index Terms—Twist, sensing, uncoupled multi-core fiber, distributed sensors, polarization-based distributed sensors, spin, birefringence.

I. INTRODUCTION

IN recent years, optical fiber sensors (OFSs) have attracted increasing research interest due to their unique advantages compared to conventional sensors, including resistance to harsh environmental conditions, flexibility, small size, and immunity to electromagnetic interference [1], [2]. Among the different types of OFSs, distributed optical fiber sensors

(DOFSs) enable continuous lengthwise measurements of physical parameters, such as temperature and strain [3], [4]; this feature is unparalleled by any other sensing technologies. To achieve distributed measurements, DOFSs leverage one of the scattering processes occurring in optical fibers, i.e., Brillouin, Raman, and Rayleigh scattering. While the majority of DOFSs are based on observing variations of either amplitude, frequency, or phase of the backscattered light, a less explored yet equally promising DOFS implementation relies on the observation of the state of polarization (SOP) of the backscattered light. The working principle of polarization-based DOFSs is based on the fact that any slight perturbation breaking the cylindrical symmetry of the fiber manifests in the form of birefringence, causing polarization variations in the propagating light [5], [6]. By measuring the SOP variations along the fiber, one can retrieve quantitative information on local perturbations; this concept has been successfully applied in Refs. [7]–[9], where the SOP variations of the Rayleigh backscattered light along single-mode fibers (SMFs) have been determined using the polarization-sensitive reflectometry technique. Notably, the SOP of light is not only sensitive to temperature and strain but it also exhibits the unique capability of being sensitive to twists [10], magnetic fields [11], and electrical currents [12]; thereby, enabling a wider range of potential applications.

Despite its unique capabilities, distributed polarization sensing (DPS) has not yet found widespread commercial applications. One of the factors hindering DPS is due to the common practice of spinning SMFs to mitigate the effect of polarization mode dispersion in optical communication systems [13], [14]. The spinning process can be described by a function that defines the fiber rotation angle – as a function of distance – while it is drawn. It has been shown that spin functions with variable spin rates, such as sinusoidal functions, are more effective in reducing polarization mode dispersion [15]; yet, variable spin rates give rise to a peculiar SOP evolution. Specifically, when the spin rate is at its maximum, the SOP undergoes fast and faint oscillations, whereas when the spin rate is close to zero, the SOP rotates around the birefringence vector, as commonly occurs in unspun fibers. On the one hand, this SOP evolution is beneficial for reducing the average

Manuscript received December XXX, 2023; revised February XXX, 2024 and March XXX, 2024.

A. Aitkulov, M. Cappelletti, D. Orsuti and L. Schenato are with the Department of Information Engineering, University of Padova, 35131 Padova, Italy (e-mail: arman.aitkulov@phd.unipd.it).

M. Santagiustina, A. Galtarossa and L. Palmieri are with the Department of Information Engineering, University of Padova, 35131 Padova, Italy, and also with National Inter-University Consortium for Telecommunications - CNIT, 43124 Parma, Italy.

T. Hayashi is with Sumitomo Electric Industries, Ltd., 1, Taya-cho, Sakae-ku, Yokohama, Kanagawa, 244-8588, Japan.

[†] These authors contributed equally to this work

The authors acknowledge partial support from the European Union under the Italian National Recovery and Resilience Plan (NRRP) of NextGenerationEU, partnership on "Telecommunications of the Future" (PE0000001 - program "RESTART") and MIUR (Project PRIN – 2022HFWMP - Debris Phos). The authors also acknowledge C. Antonelli and A. Mecozzi from the University of L'Aquila for providing the fan in/out.

birefringence strength in optical communication systems; on the other hand, it poses a challenge for DPS because a high spatial resolution and SOP accuracy are required to track the evolution of the local birefringence vector. For this reason, DPS is commonly implemented with optical frequency domain reflectometry (OFDR) to achieve high spatial resolution, typically in the order of a few micrometers, at the expense of a limited measurement range of a few tens of meters [16].

Recently, new classes of optical fibers have been developed in the context of spatial-division multiplexed transmission systems [17], [18]. This made multi-core fibers (MCFs) become a widely accessible technology, providing new opportunities for sensing applications. Uncoupled MCFs offer two significant advantages for DPS. First, uncoupled MCFs are typically not spun because the spinning process would lead to an undesirable increase in core cross-talk. Second, uncoupled MCFs have been shown to exhibit remarkable uniformity and regularity – both in modulus and orientation – of the birefringence vector [8], making them well-suited for DPS. We remark that the above-mentioned MCFs are the standard ones designed for telecommunication purposes, easily drawable for kilometers [17], and already deployed in field trials [18]. Up until now, a few kinds of twist sensors also based on MCFs have been proposed. Yet all of the proposed solutions either are not able to perform a distributed measurement or employ non-telecom grade fiber, designed on purpose. For example, Refs. [19]–[21] report point sensors based on custom-made MCFs. Ref. [22] describes a twist sensor based on long-period grating inscribed into a special helically polished fiber. Finally, Refs. [23] and [24] report distributed twist sensors that however use very special MCFs drawn with a spin period below 1 mm.

In this work, extending a preliminary analysis reported in Ref. [25], we show that uncoupled MCFs employed for telecom applications can be used as a promising technological platform for implementing polarization-based distributed twist sensing. Specifically, we conduct polarization-sensitive OFDR measurements to determine the twist-induced birefringence along the cores of an uncoupled four-core fiber (U4CF). By applying a controlled twist to the fiber, we show that the elasto-optic rotation coefficient of each core is consistent with the previously reported value for SMFs. Moreover, we demonstrate that the measured twist matches the nominally applied one even when the U4CF is perturbed at a distance of 500 meters from the source. The angle by which the fiber is twisted can be measured with a remarkable accuracy of 4° and with a spatial resolution of 8 cm. The achieved performance makes U4CF a promising technological platform for applications in fields such as umbilical cable monitoring and robotics [23].

The paper is organized as follows. Section II elaborates on the twist effects on UMCFs. Section III reviews the principle of twist measurements using the polarization-sensitive reflectometry technique. Section IV presents the experimental setup used in this work. Section V assesses and discusses the performance of the sensor over different twist combinations.

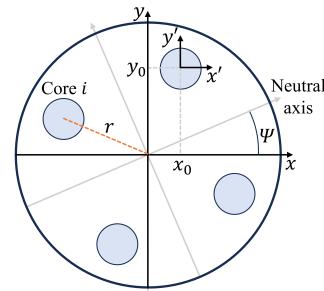


Fig. 1. Schematic cross-section of U4CF showing the arrangement of the cores.

II. TWIST EFFECTS ON UNCOUPLED MULTI-CORE FIBERS

In contrast to SMFs, where the core is centered on the fiber axis, cores in a MCF are symmetrically arranged around the fiber axis. Therefore, to develop a twist sensor based on MCFs, it is crucial to understand the effect of twist on the field propagating in the offset cores, as well as the impact of twist on the birefringence of each offset core.

To determine the stress field induced on the cores due to twist, we rely on coupled mode theory [26], [27]. In each core, the evolution of the complex amplitude, a_μ , of a specific mode μ propagating along the z -axis is governed by the equation

$$\frac{da_\mu}{dz} = -jC_\mu a_\mu(z) - j \sum_\nu K_{\mu,\nu}(z) a_\nu(z), \quad (1)$$

where C_μ is the propagation constant of mode μ , and $K_{\mu,\nu}$ denotes the coupling coefficients influenced by perturbations acting on the core. These coefficients can be determined through the integrals [26]

$$K_{\mu,\nu} = \frac{\omega}{4} \iint \mathbf{E}_\mu^*(\mathbf{x}'_t) \delta\epsilon(\mathbf{x}'_t, z) \mathbf{E}_\nu(\mathbf{x}'_t) d\mathbf{x}'_t, \quad (2)$$

where $\delta\epsilon(\mathbf{x}'_t, z)$ is a 3×3 matrix denoting the perturbation term added to the dielectric tensor of the ideal fiber core to obtain the perturbed one; the vector \mathbf{x}'_t defined as

$$\mathbf{x}'_t = \begin{bmatrix} x' \\ y' \end{bmatrix} = \begin{bmatrix} x - x_0 \\ y - y_0 \end{bmatrix}, \quad (3)$$

spans the fiber section and provides the position of a generic core relative to the fiber axis (see Fig. 1). The vectors $\mathbf{E}_\mu(\mathbf{x}'_t)$ and $\mathbf{E}_\nu(\mathbf{x}'_t)$ denote the transverse components of electric fields for modes μ and ν , respectively. When a core is twisted by an angle $\psi(z)$, shear stresses are applied to the silica material, resulting in an elasto-optic effect that introduces a perturbation $\delta\epsilon_{\text{twist}}$ in the permittivity tensor that can be written as [15], [27]

$$\delta\epsilon_{\text{twist}}(\mathbf{x}_t, z) = \epsilon_0 n_{\text{av}}^2 g \tau(z) \begin{bmatrix} 0 & 0 & -y \\ 0 & 0 & x \\ -y & x & 0 \end{bmatrix}, \quad (4)$$

where ϵ_0 is the vacuum permittivity, n_{av} denotes the average refractive index, $g \simeq 0.144$ is the elasto-optic coefficient [28], and $\tau(z) = d\psi/dz$ is the applied twist rate. Interestingly, due to the symmetries inherent in the fundamental modes, direct inspection of Eq. (2) indicates that the offset positions of the

cores do not contribute to the value of $K_{\mu,\nu}$. Consequently, although the stress field induced by twist is not uniform, its electromagnetic impact on the cores remains independent of their positions. This means that the effect of the twist on each core is the same as that observed in SMFs; it consists in the rotation of the core intrinsic linear birefringence by the twist angle ψ and in the generation of torsional-stress circular birefringence proportional to the twist rate applied τ , according to $-g\tau$.

To understand the impact of twist on the birefringence of each core, we can rely on the following geometrical considerations. When the UMCF is twisted, the cores follow a helical trajectory; therefore, the torsion of the helix is in principle different from that applied to the fiber axis. Nonetheless, the distance from the fiber axis to a specific core, r , is many orders of magnitudes smaller than the helix pitch, p , induced by twist; typical order of magnitudes are micrometers and centimeters, respectively. Therefore, the torsion of the helix, $p/(r^2 + p^2)$, can be very well approximated by $1/p$, which corresponds to the actual twist applied to the fiber. Consequently, each core of the MCF undergoes the same variations of the local birefringence angle in the presence of a twist.

It is worth mentioning that while in this section we focus on the twist effects, in practical scenarios, the fiber is subject to both twist and bending. However, the effect of bending on birefringence has been shown to be negligible, except for bending radii smaller than a few centimeters [9], [29]. Such tight bends are not common, especially in applications like twist monitoring of umbilical power lines, where the inherent rigidity of the cable prevents extreme bending. Consequently, the effect of bending can be safely neglected in our analysis.

III. POLARIZATION-RESOLVED TWIST MEASUREMENTS

A practical approach to measure the local birefringence variation induced by twist is polarization-sensitive reflectometry. However, the polarization of the backscattered light is not directly related to the local properties of the fiber; instead, it is affected by the entire round-trip propagation [16]. Consequently, an inverse scattering problem must be solved to extract information about the local birefringence. In this section, we recall the key points of the technique, while referring the reader to Refs. [7], [30] for a comprehensive discussion.

The evolution of the SOP, $\hat{s}(z)$, in a generic core can be described as $d\hat{s}/dz = \bar{\beta} \times \hat{s}$, where $\bar{\beta}(z)$ denotes the birefringence vector that we aim to measure. The vector $\bar{\beta}(z)$ can be expressed as $\bar{\beta}(z) = (\beta_L \cos 2\theta, \beta_L \sin 2\theta, \beta_C)^T$, where the first two components are the linear part of birefringence, and β_C is the circular birefringence, which is only due to the twist (Faraday rotation apart [16]). In the above expression, $\theta(z)$ denotes the cumulative rotation of birefringence up to the position z , which can be due to both the intrinsic random orientation along the core and the deterministic effect of twist.

As anticipated, a polarization-sensitive reflectometer measures the backscattered SOP, $\hat{s}_B(z)$, whose evolution is gov-

erned by the equation

$$\frac{d\hat{s}_B}{dz} = \bar{\beta}_B(z) \times \hat{s}_B(z). \quad (5)$$

where $\bar{\beta}_B(z)$ is the round-trip birefringence. Analogously to $\bar{\beta}$, $\bar{\beta}_B$ is also affected by the perturbations applied to the fiber, yet the relation between the two quantities is not straightforward. It can be shown that $\bar{\beta}_B(z) = 2\mathbf{B}(z)\bar{\beta}_A(z)$ [16], where the factor 2 accounts for round-trip propagation, $\mathbf{B}(z)$ denotes the Mueller matrix representing backward propagation from a position z to the fiber input, and $\bar{\beta}_A(z)$ is the so-called "apparent" birefringence, which is related to the "real" local birefringence of the core $\bar{\beta}$. The apparent birefringence can be written as [28]

$$\begin{aligned} \bar{\beta}_A(z) &= \beta_L(\cos 2\phi, \sin 2\phi, 0)^T, \\ \phi(z) &= \theta(z) - \frac{1}{2} \int_0^z \beta_C(u) du, \end{aligned} \quad (6)$$

showing that the circular birefringence induced by the twist is measured by a polarization-sensitive reflectometer as an apparent rotation of the linear part. Eq. (6) is the core of DPS-based twist measurements. Note that, to extract information about the twist, the angle $\theta(z)$ must be known; it can be obtained by performing a reference measurement at the beginning of the sensing session.

Based on the above theory, we determine the angle by which the fiber is twisted as follows. We measure the backscattered SOP \hat{s}_B , with a polarization-sensitive reflectometer. Next, we compute the round-trip birefringence $\bar{\beta}_B$; this step can be achieved by probing the fiber with at least two input SOPs and estimating $\bar{\beta}_B$ with known algorithms [31], [32]. Then, we compute the Mueller matrix of the backward propagation by numerically solving the differential equation

$$\frac{d\mathbf{B}}{dz} = \frac{1}{2} \cdot \bar{\beta}_B(z) \times \mathbf{B}(z), \quad (7)$$

and we calculate the apparent birefringence as

$$\bar{\beta}_A(z) = \frac{1}{2} \cdot \mathbf{B}^T(z) \cdot \bar{\beta}_B(z), \quad (8)$$

from which the angle $\phi(z)$ can be determined. When the fiber is twisted by an angle $\psi(z)$, the deterministic effect of twist adds up to the intrinsic random rotation of birefringence, $\theta(z)$, as [28]

$$\phi(z) = \theta(z) + \left(1 - \frac{g}{2}\right) \psi(z), \quad (9)$$

so we determine $\psi(z)$ by removing the angle $\theta(z)$, which is obtained from the reference measurement without induced twist. Fig. 2 shows an example of the components of the apparent birefringence vector ($\bar{\beta}_A$) measured in one of the cores of the MCF when this fiber was deployed almost straight on the floor. As expected from the theoretical model, the third component is almost zero, confirming the good quality of the measurement. At the same time, the linear component of the $\bar{\beta}_A$ (i.e., the first two elements of the vector) shows a random variation. Correspondingly, Fig. 3 shows the modulus and angle of this linear component; both quantities have a rather regular behavior, quite different from that of SMFs where typically the modulus is Rayleigh distributed and the

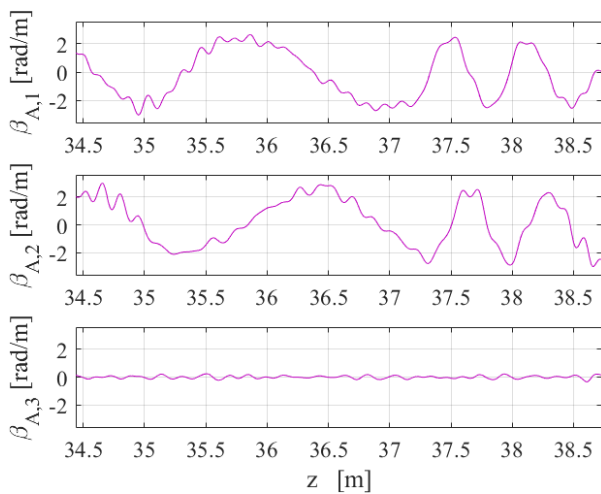


Fig. 2. Apparent birefringence vector components of one of the cores of the U4CF.

angle varies as a Wiener random process [10]. This difference is the main reason why DPS measurements are effective in MCFs.

The twist range of this technique depends on the ability to measure the spatial variation of the backscattered SOP; hence, it depends on the spatial resolution, δz , and the birefringence strength, β . This dependence is non-trivial, and details can be found in Ref. [33]. However, when the spatial resolution is much smaller than the beat length, $L_B = 2\pi/\beta$, the maximum measurable twist rate is approximately equal to

$$\tau_{max} \approx \frac{\pi}{2\delta z}. \quad (10)$$

IV. EXPERIMENTAL SETUP

To obtain the backscattered SOP, $\hat{s}_B(z)$, along the core of the U4CF, the interrogation setup must set the SOP of the probe light without affecting the SOP of the backscattered light. This can be achieved through the setup shown

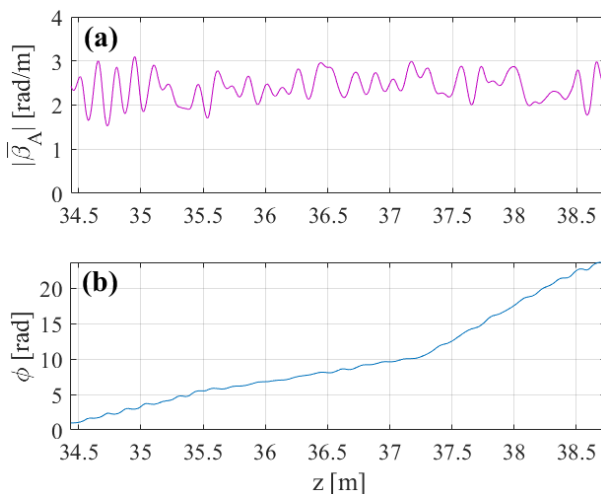


Fig. 3. (a) Modulus and (b) angle of linear component of apparent birefringence in one of the cores of the straight fiber.

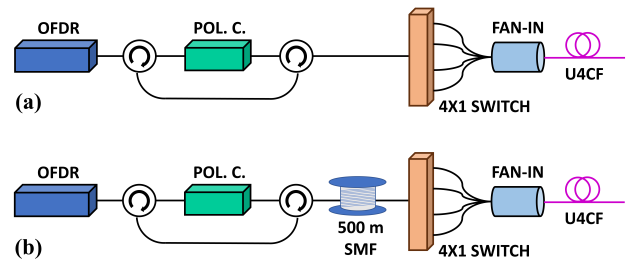


Fig. 4. Experimental setup for backscattered SOP measurements. The U4CF is probed (a) directly, and (b) after propagating over 500 m of SMF.

in Fig. 4(a), which consists of a commercial OFDR (Luna OBR 4600), two circulators, and a polarization controller to set the desired SOP of the probe light. An optical switch is employed to select a specific core of the U4CF and a fan-in device (Optoscribe; 3D Optofan series) is used to couple the switch outputs to the cores. The time needed to perform the measurement is mainly determined by the OFDR scan, which is several orders of magnitude longer than the switching time of the fan-in device. Nonetheless, it should be noted that each core experiences the same twist; therefore, if speed is the main concern, the measurement can be limited to one core. The fiber under test has a core pitch of $40 \mu\text{m}$ and the cores are arranged at the vertices of a square; further specifications about the fiber can be found in Ref. [17]. In principle, as stated in Section III, it is sufficient to probe the cores with two different input SOPs to estimate $\hat{\beta}_B(z)$; however, in our experiment, we launch four different input SOPs to increase the accuracy of the estimate [34]. We investigate the sensor performance over the two experimental configurations shown in Figs. 4 (a) and (b), differing in the total length of the fiber link. In the first configuration [Fig. 4(a)], the 7-m-long U4CF fiber is probed directly; in this case, the OFDR scans a bandwidth of 43 nm around 1550 nm, yielding a spatial resolution of about $20 \mu\text{m}$. In the second configuration [Fig. 4 (b)], the U4CF is probed at a distance of 500 m from the OFDR source to investigate the performance in a more realistic scenario. Due to the lack of a sufficiently long U4CF sample in our laboratory, we insert a 500 m-long G.652 standard SMF between the OFDR source and the fan-in connecting the switch with the U4CF. Note that this choice does not compromise the validity of the analysis since the objective is to investigate the sensor performance with a coarser spatial resolution of the OFDR measurement, regardless of which fiber – SMF or MCF – connects the interrogation setup with the U4CF. With the 500 m-long fiber inserted, the limitations posed by the laser coherence length force the OFDR system to scan a narrower bandwidth of 0.8 nm, namely 50 times smaller compared to direct probing; yielding a spatial resolution of about 1 mm. The maximum theoretical length is dictated by the dynamic range of the specific OFDR device used to perform the measurements, which is 2 km for the device used here. Longer distances can be potentially achieved with phase-compensated OFDR or P-OTDR; in this case, however, the effect of the cumulated PMD should also be taken into consideration.

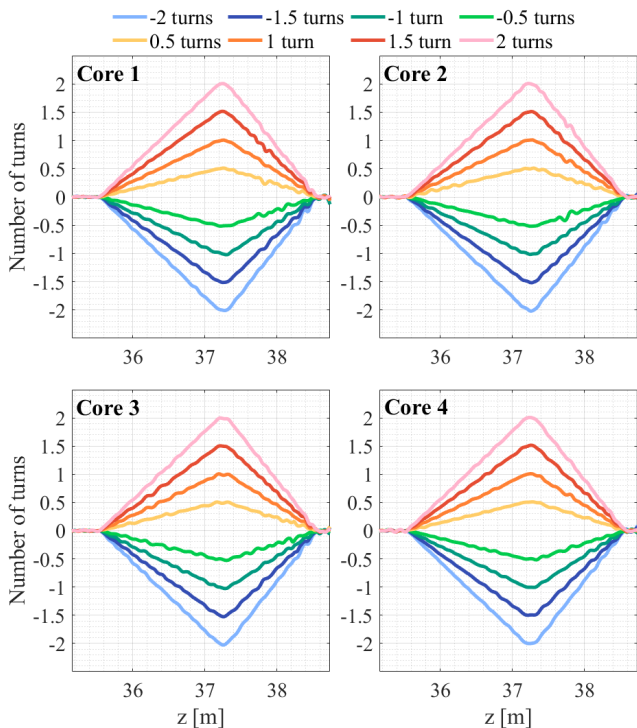


Fig. 5. Variations in the orientation of the birefringence vector with respect to the reference measurement for all the cores of the U4CF. The measurements have been performed with the setup shown in Fig. 4(a). The legend indicates the number of turns applied to the fiber at the position $z = 37.3$ m; "+" represents clockwise rotation, and "-" represents counterclockwise rotation. The plotted curves accurately capture the local twist applied to the fiber.

V. RESULTS AND DISCUSSION

To validate that the elasto-optic coefficient, g , of each core is consistent with the one of SMFs, and that the offset cores experience the same variation of local birefringence when twist is applied (see Section II), we conduct the following experiment. We consider the setup shown in Fig. 4(a), and deploy the U4CF along a straight path; in this unperturbed configuration, we measure the random orientation of birefringence along the cores, serving as a reference for subsequent measurements. Next, we fix the fiber in two points, 3 meters apart, and apply a controlled twist by rotating the fiber around its axis at a point between the two fixed ones. We measure the local birefringence while varying the number of turns from -2 to 2 in increments of 0.5 . The results of this experiment, calculated assuming $g = 0.144$ for each core (as in SMF [16]), are shown in Fig. 5. The plotted curves accurately track the local twist applied to the fiber. The triangle-shaped curves are due to the fact that the fiber sections before and after the point where the twist is applied, i.e., $z = 37.3$ m, undergo rotations with different twist rate, ranging from 3.15 to 12.6 rad/m, and with opposite helicity. To obtain the results shown in Fig. 5, the backscattered SOP has been low-pass filtered so to increase the signal-to-noise ratio by reducing the impact of Rayleigh fading noise (see Section 3.2 in Ref. [4]); such filtering process worsen the spatial resolution from $20 \mu\text{m}$ (given by the OFDR measurement) to 6 cm, which is the effective spatial resolution after data analysis. The spatial resolution can be improved by

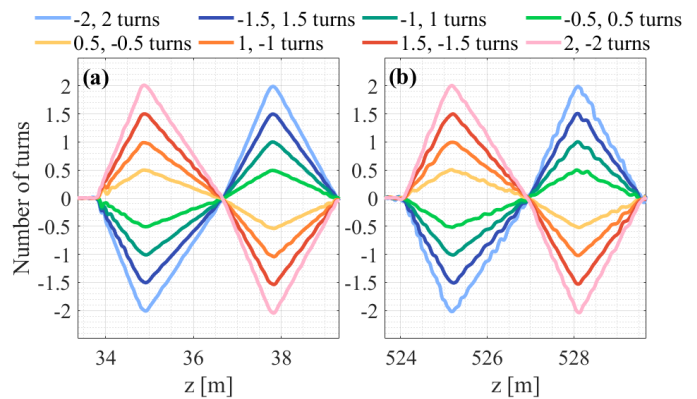


Fig. 6. Variations in the orientation of the birefringence vector with respect to the reference measurement when two twists with same amplitude but different directions are applied to the U4CF; (a) when the fiber is probed directly, and (b) after propagating 500 m from the source. The twists applied at the positions [referring to (a)] $z_1 = 34.9$ m and $z_2 = 37.8$ m, respectively, are specified in the legend.

adjusting the filter parameters, which, however, also affect the SNR value. Thus, a compromise between the accuracy and the SNR has to be maintained. According to Eq. 10, given that $\beta \approx 2.5$ rad/m (see Fig. 3(a)), a spatial resolution of 6 cm yields a maximum measurable twist rate of about 26.2 rad/m.

To demonstrate the feasibility of distributed twist measurement at long range, we compare the sensing performance between the setup configuration shown in Fig. 4(a) and (b). In this experiment, the fiber is fixed at three points each separated by about 2.5 m, and we apply two twists, equal in amplitude but opposite in direction. The results are shown in Fig. 6, where we plot the results for a single core only since, as demonstrated above, the other cores experience analogous local birefringence variations.

Remarkably, the results show that the local twist applied to the fiber can be obtained, both when the fiber is probed directly [Fig. 6(a)] and when it is probed after propagating over 500 m of SMF [Fig. 6(b)]. The effective spatial resolution after filtering the SOPs is of 6 cm and 8 cm for the short and long configuration, respectively, corresponding to maximum measurable twist rates of 26.2 rad/m and 19.6 rad/m. The oscillations in the curves of Fig. 6(b) are due to the poorer spatial resolution of the measurements, which results in a lower accuracy when applying numerical integration algorithms in the data analysis. Nonetheless, the measured twist is well in agreement with the one applied to the fiber.

Figure 7 shows the sensor performance when the applied twists have both different amplitudes and different directions; the following combinations of twists are applied: 1 and 0 turns, 2 and -1 turns, -1.5 and -0.5 turns, -0.5 and 1 turns. The results show accurate detection of the induced twist for both configurations.

To determine the noise floor of the sensor, we deploy the fiber in a straight path while minimizing the induced twist. Next, we perform repeated measurements of the backscattered SOP at different time instants. We consider as a reference the

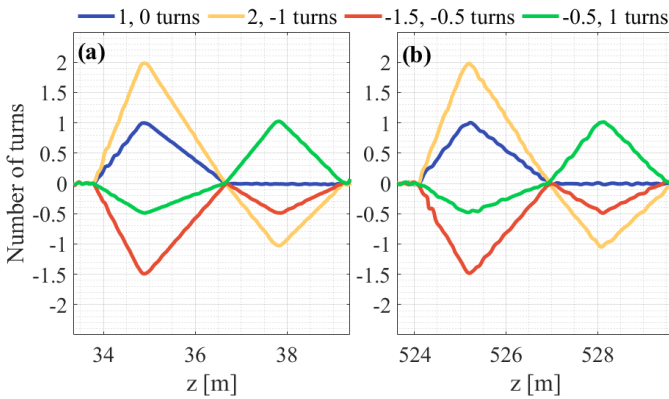


Fig. 7. Variations in the orientation of the birefringence vector with respect to the reference measurement when two twists with both different amplitude and different directions are applied to the U4CF; (a) when the fiber is probed directly, and (b) after propagating 500 m from the source. The twists applied at the positions $z = 34.9$ m and $z = 37.8$ m, respectively, are specified in the legend.

average birefringence orientation computed as

$$\bar{\phi}(z) = \frac{1}{N} \sum_{n=1}^N \phi_n(z) \quad (11)$$

where N is the number of repeated measurements. We use this reference angle to compute the birefringence variations for the subsequent measurements; in these settings, any variation of the local birefringence orientation can be attributed to noise. The results of this analysis for an ensemble of six measurements are shown in Fig. 8, where we plot the probability density function (PDF) of the noise signal when the fiber is probed directly (dashed blue line) and after propagating through the 500-m-long link (dashed red line). The standard deviations are 0.003 and 0.011 turns for direct probing and long-range probing, respectively. As expected, the long-range setup configuration leads to a higher noise floor value with an increase of 0.008 turns, i.e., about 3° . Nonetheless, the sensor enables detecting rotation variations as low as 4° , which is relevant for many applications.

It is also interesting to evaluate the repeatability of the measured twist; to achieve this, we proceed analogously to the above analysis, but with the fiber twisted as in the config-

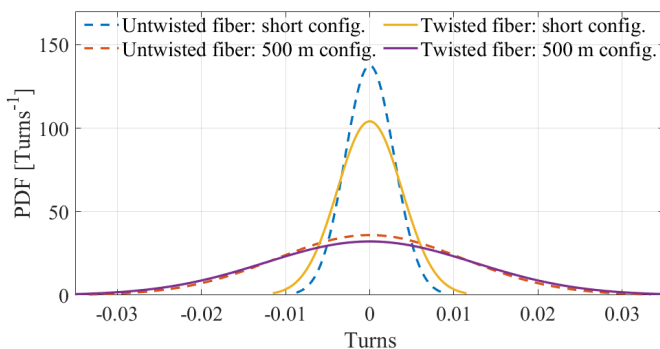


Fig. 8. Probability density function of the noise floor of the sensor evaluated for the configurations shown in the legend. The curves are obtained analyzing an ensemble of 6 measurements.

uration shown in Fig. 6 with 1.5 turns in the positive direction. In this case, the standard deviation values are approximately 0.004 and 0.012 turns, for the direct probing (yellow solid line in Fig. 8) and long-range probing (purple solid line), respectively. The increase in the standard deviation in the twisted fiber can be attributed to the twist itself, which causes a faster variation of the SOP, bringing the measurement closer to the spatial resolution limit. Still, as before, the noise floor value increases by a low value of about 3° across the two configurations.

This uncertainty can be imputed mostly to measurement noise, including Rayleigh fading noise. Other possible sources of uncertainty could, in principle, be a drift with respect to the reference. In particular, one source of drift could be a variation of birefringence not related to twist, such as, for example, bending. Nevertheless, since the bending birefringence is proportional to the square curvature [9], [29], it is sufficient to keep bending radii above some centimeters to avoid this effect.

A possible second source of drift is the temperature dependence of the elasto-optic coefficient g . However, according to Ref. [35], the temperature coefficient can be estimated in $\frac{dg}{dT} \approx 1.8 \times 10^{-4} K^{-1}$. This means that even a variation of a few tens of Kelvins would induce a drift that is negligible compared to the noise floor of the measurement.

VI. CONCLUSION

We investigated the performance of distributed twist sensing over standard uncoupled multi-core fibers deployed for telecom applications. In contrast to standard single-mode fibers, uncoupled multi-core fibers are not spun to avoid increasing the core crosstalk. For this reason, they offer interesting birefringence properties. Through polarization-sensitive OFDR, we demonstrated that twist-induced birefringence can be accurately measured along the cores of the U4CF. By applying a controlled twist to the fiber, we determined that elasto-optic rotation coefficient of each core is consistent with the one known in the literature for SMFs. We also showed that the cores experience the same variations in birefringence in presence of twist. Throughout the experiments, we considered two setup configurations differing by the fiber link length. The first setup probes the U4CF directly, and the second setup interrogates the U4CF that is 500 m away from the source along the probed path, so as to investigate the possibility of long-range twist sensing. In the latter case, the OFDR operated with a scan bandwidth 50 times smaller compared to the short configuration, while still enabling to recover the nominally applied twist with an accuracy of 4° in the angle by which the fiber is twisted and a spatial resolution of 8 cm. The proposed UMCF-based twist sensor stands as a reliable solution for applications like umbilical cable monitoring, where the ability to accurately monitor twists along a cable is crucial to avoid cable failure.

REFERENCES

- [1] B. Culshaw and A. Kersey, "Fiber-optic sensing: A historical perspective," *J. Lightwave Technol.*, vol. 26, no. 9, pp. 1064–1078, 2008.

- [2] J. M. López-Higuera, *Handbook of Optical Fibre Sensing Technology*. Wiley, 2002.
- [3] A. H. Hartog, *An Introduction to Distributed Optical Fibre Sensors*. CRC press, 2017.
- [4] L. Palmieri, L. Schenato, M. Santagiustina, and A. Galtarossa, "Rayleigh-based distributed optical fiber sensing," *Sensors*, vol. 22, no. 18, 2022.
- [5] R. Ulrich and A. Simon, "Polarization optics of twisted single-mode fibers," *Appl. Opt.*, vol. 18, no. 13, pp. 2241–2251, Jul. 1979.
- [6] L. Palmieri, M. Cappelletti, M. Santagiustina, and A. Galtarossa, "Polarization-dependent phase of light propagating in optical fibers," *J. Lightwave Technol.*, vol. 41, no. 21, pp. 6786–6794, 2023.
- [7] L. Palmieri, "Distributed polarimetric measurements for optical fiber sensing," *Opt. Fiber Technol.*, vol. 19, no. 6, pp. 720–728, Dec. 2013.
- [8] R. Veronese, C. Antonelli, A. Mecozzi, T. Hayashi, M. Santagiustina, A. Galtarossa, and L. Palmieri, "Distributed measurement of birefringence in uncoupled multicore fibers," in *Optical Fiber Communication Conference (OFC) 2021*. Optica Publishing Group, 2021, p. W7B.3.
- [9] L. Palmieri, A. Galtarossa, and T. Geisler, "Distributed characterization of bending effects on the birefringence of single-mode optical fibers," *Opt. Lett.*, vol. 35, no. 14, pp. 2481–2483, Jul. 2010.
- [10] A. Galtarossa and L. Palmieri, "Measure of twist-induced circular birefringence in long single-mode fibers: Theory and experiments," *J. Lightwave Technol.*, vol. 20, no. 7, p. 1149, Jul. 2002.
- [11] L. Palmieri and A. Galtarossa, "Distributed fiber optic sensor for mapping of intense magnetic fields based on polarization sensitive reflectometry," in *Third Asia Pacific Optical Sensors Conference*, J. Canning and G. Peng, Eds., vol. 8351, International Society for Optics and Photonics. SPIE, 2012, p. 835131.
- [12] L. Palmieri, D. Sarchi, and A. Galtarossa, "Distributed measurement of high electric current by means of polarimetric optical fiber sensor," *Opt. Express*, vol. 23, no. 9, pp. 11073–11079, May 2015.
- [13] A. J. Barlow, J. J. Ramskov-Hansen, and D. N. Payne, "Birefringence and polarization mode-dispersion in spun single-mode fibers," *Appl. Opt.*, vol. 20, no. 17, pp. 2962–2968, Sep. 1981.
- [14] L. Palmieri, "Polarization properties of spun single-mode fibers," *J. Lightwave Technol.*, vol. 24, no. 11, pp. 4075–4088, Nov. 2006.
- [15] A. Galtarossa, L. Palmieri, and D. Sarchi, "Measure of spin period in randomly birefringent low-PMD fibers," *IEEE Photon. Technol. Lett.*, vol. 16, no. 4, pp. 1131–1133, 2004.
- [16] A. Galtarossa, D. Grosso, L. Palmieri, and M. Rizzo, "Spin-profile characterization in randomly birefringent spun fibers by means of frequency-domain reflectometry," *Opt. Lett.*, vol. 34, no. 7, pp. 1078–1080, Apr. 2009.
- [17] T. Hayashi, "Multi-core fiber technology from design to deployment," in *2022 European Conference on Optical Communication (ECOC)*, 2022, pp. 1–4.
- [18] B. J. Puttnam, G. Rademacher, and R. S. Luís, "Space-division multiplexing for optical fiber communications," *Optica*, vol. 8, no. 9, pp. 1186–1203, Sep. 2021.
- [19] P. Xue, Q. Liu, Q. Wu, and Y. Fu, "The fabrication of an eccentric three-core fiber and its application as a twist sensor," *IEEE Transactions on Instrumentation and Measurement*, vol. 71, pp. 1–6, 2022.
- [20] T. Cheng, B. Li, F. Zhang, W. Liu, X. Chen, Y. Gao, X. Yan, X. Zhang, F. Wang, T. Suzuki, and Y. Ohishi, "A sagnac interferometer-based twist angle sensor drawing on an eccentric dual-core fiber," *IEEE Transactions on Instrumentation and Measurement*, vol. 71, pp. 1–8, 2022.
- [21] W. Luo, Y. Chen, A. Xiao, Q. Ling, B. Zhang, S. Luo, Z. Yu, Y. Zhang, Z. Guan, and D. Chen, "Three-core fiber-based temperature-insensitive twist sensor," *Opt. Commun.*, vol. 554, p. 130229, 2024.
- [22] C. Sun, R. Wang, X. Jin, W. Liu, X. Chen, S. Zhang, Q. Zhu, L. Chen, Y. Zhang, K. Zhang, T. Geng, C. Tong, Z. Qu, and L. Yuan, "A novel twist sensor based on long-period fiber grating written in side-helical polished structure," *IEEE Photon. Technol. Lett.*, vol. 32, no. 5, pp. 275–278, 2020.
- [23] G. Yin, L. Lu, L. Zhou, C. Shao, Q. Fu, J. Zhang, and T. Zhu, "Distributed directional torsion sensing based on an optical frequency domain reflectometer and a helical multicore fiber," *Opt. Express*, vol. 28, no. 11, pp. 16140–16150, May 2020.
- [24] C. Chen, Z. Zhao, Z. Lin, Y. Yao, Y. Xiong, W. Tong, and M. Tang, "Distributed twist sensing using frequency-scanning ϕ -OTDR in a spun fiber," *Opt. Express*, vol. 31, no. 11, pp. 17809–17819, May 2023.
- [25] D. Orsuti, A. Aitkulov, M. Cappelletti, L. Schenato, M. Magarotto, M. Santagiustina, C. Antonelli, A. Mecozzi, T. Hayashi, A. Galtarossa, and L. Palmieri, "Multi-core fibers as a technological platform for distributed twist sensing," in *28th International Conference on Optical Fiber Sensors*, 2023.
- [26] D. Marcuse, "Coupled-mode theory for anisotropic optical waveguides," *The Bell System Technical Journal*, vol. 54, no. 6, pp. 985–995, 1975.
- [27] L. Palmieri and A. Galtarossa, "Coupling effects among degenerate modes in multimode optical fibers," *IEEE Photonics J.*, vol. 6, no. 6, pp. 1–8, 2014.
- [28] A. Galtarossa, D. Grosso, and L. Palmieri, "Accurate characterization of twist-induced optical activity in single-mode fibers by means of polarization-sensitive reflectometry," *IEEE Photon. Technol. Lett.*, vol. 21, no. 22, pp. 1713–1715, 2009.
- [29] M. Cappelletti, D. Orsuti, M. H. Vandborg, A. Aitkulov, P. D. Olmo, L. Schenato, M. Magarotto, M. Santagiustina, C. Antonelli, A. Mecozzi, T. Hayashi, L. Grüner-Nielsen, L. S. Rishøj, K. Rottwitt, A. Galtarossa, and L. Palmieri, "Preliminary analysis of polarization effects in bent uncoupled-core multicore fibers," in *28th International Conference on Optical Fiber Sensors*, 2023.
- [30] A. Galtarossa, D. Grosso, L. Palmieri, and L. Schenato, "Reflectometric measurement of birefringence rotation in single-mode optical fibers," *Opt. Lett.*, vol. 33, no. 20, pp. 2284–2286, Oct. 2008.
- [31] K. Kanatani, "Analysis of 3-D rotation fitting," *IEEE Transactions on Pattern Analysis and Machine Intelligence*, vol. 16, no. 5, pp. 543–549, 1994.
- [32] R. Jopson, L. Nelson, and H. Kogelnik, "Measurement of second-order polarization-mode dispersion vectors in optical fibers," *IEEE Photon. Technol. Lett.*, vol. 11, no. 9, pp. 1153–1155, 1999.
- [33] L. Palmieri, T. Geisler, and A. Galtarossa, "Limits of applicability of polarization sensitive reflectometry," *Opt. Express*, vol. 19, no. 11, pp. 10874–10879, May 2011.
- [34] P. Phua, J. Fini, and H. Haus, "Real-time first- and second-order PMD characterization using averaged state-of-polarization of filtered signal and polarization scrambling," *J. Lightwave Technol.*, vol. 21, no. 4, pp. 982–989, 2003.
- [35] A. M. Smith, "Birefringence induced by bends and twists in single-mode optical fiber," *Appl. Opt.*, vol. 19, no. 15, pp. 2606–2611, Aug. 1980.